

Modeling PET Data Acquired During Nonsteady Conditions: What If Brain Conditions Change During the Scan?

Evan D. Morris^{1–3}, Gaele M. Emvalomenos⁴, Jocelyn Hoye³, and Steven R. Meikle^{4,5}

¹Radiology and Biomedical Imaging, Yale University, New Haven, Connecticut; ²Biomedical Engineering, Yale University, New Haven, Connecticut; ³Psychiatry, Yale University, New Haven, Connecticut; ⁴Faculty of Medicine and Health, University of Sydney, Sydney, Australia; and ⁵Sydney Imaging Core Research Facility, University of Sydney, Sydney, Australia

Researchers use dynamic PET imaging with target-selective tracer molecules to probe molecular processes. Kinetic models have been developed to describe these processes. The models are typically fitted to the measured PET data with the assumption that the brain is in a steady-state condition for the duration of the scan. The end results are quantitative parameters that characterize the molecular processes. The most common kinetic modeling endpoints are estimates of volume of distribution or the binding potential of a tracer. If the steady state is violated during the scanning period, the standard kinetic models may not apply. To address this issue, time-variant kinetic models have been developed for the characterization of dynamic PET data acquired while significant changes (e.g., short-lived neurotransmitter changes) are occurring in brain processes. These models are intended to extract a transient signal from data. This work in the PET field dates back at least to the 1990s. As interest has grown in imaging nonsteady events, development and refinement of time-variant models has accelerated. These new models, which we classify as belonging to the first, second, or third generation according to their innovation, have used the latest progress in mathematics, image processing, artificial intelligence, and statistics to improve the sensitivity and performance of the earliest practical time-variant models to detect and describe nonsteady phenomena. This review provides a detailed overview of the history of time-variant models in PET. It puts key advancements in the field into historical and scientific context. The sum total of the methods is an ongoing attempt to better understand the nature and implications of neurotransmitter fluctuations and other brief neurochemical phenomena.

Key Words: radiotracer tissue kinetics; lp-ntPET; neurotransmitter; time-varying models; tracer kinetics; transient signal

J Nucl Med 2024; 00:1–14

DOI: 10.2967/jnumed.124.267494

Researchers use PET imaging with target-selective tracer molecules to probe brain physiology by calculating the strength or weakness of critical molecular processes. Often, the goal is to observe the brain's steady state functioning (e.g., the concentration of enzymes, receptors, or cells of a certain type). From a modeling standpoint, the steady state is characterized by macroparameters quantifying important characteristics of brain function that do not

change from minute to minute. The most common of these characteristics includes the volume of distribution (V_T) of a tracer molecule (i.e., the carrying capacity of a tissue for that molecule [Table 1] summarizes variables used in the text) or the binding potential (BP) of a tracer (i.e., the steady-state ratio of the density of a molecule's binding sites to its affinity for those sites). PET is often the tool of choice for revealing the workings of the living brain as they occur in the world. To conduct a PET experiment on a human subject, we require the subject to lie still in an unfamiliar, sterile environment and be injected by a stranger with a radioactive material. We do all this while assuming that the experiment itself does not alter the state of the subject's brain. Our assumption may be unrealistic. But technically, many such assumptions underlie any proper measurement of the steady state of the brain. The act of observing must not alter the observed.

In other circumstances, however, the purpose of the experiment is expressly and intentionally to perturb the steady state—that is, to alter the observed. In such circumstances, the experimental conditions are selected specifically by the investigator to temporarily increase or decrease an otherwise steady function. The intent may be to alter the available number of specific binding sites. This could be accomplished experimentally by stimulating or suppressing the amount of neurotransmitter that binds to the site. It could be done by changing the confirmation of the binding site or by altering its steady level of trafficking from the cell interior to the cell surface. Yet another type of experiment is one configured to abruptly alter brain blood flow regionally. Short-acting drugs often change the steady state of the system.

There are innumerable experiments in which studying the brain in its disturbed steady state is valuable and informative. For example, dopamine transmission is not static. A story is emerging from preclinical and clinical research that temporal patterns of dopamine transmission in response to a stimulus encode important information that may be relevant for understanding drug addiction and treatment. These patterns may differ by location. Volkow and Swanson (1) linked temporal patterns of [¹¹C]cocaine uptake—an indirect marker of elevated synaptic dopamine—to temporal patterns of subjective reports of feeling high and craving cocaine. Rapid elevation of dopamine has thus come to be associated with a fast onset of a drug high and drug craving (1). Work on this topic continues (2,3). On the basis of microdialysis work in rats, it has been hypothesized that the partial nicotinic agonist, varenicline (Chantix; Pfizer), reduces the reinforcing properties of nicotine by eliminating sharp peaks in the dopamine response to nicotine (4)—that is, by altering the temporal pattern of dopamine release. Microdialysis and PET have been used jointly to examine dopamine transmission in the cortex of monkeys, leading to claims that dopamine transmission in response to a drug

Received Jan. 23, 2024; revision accepted Sep. 11, 2024.

For correspondence or reprints, contact Evan D. Morris (evan.morris@yale.edu).

Published online Oct. 24, 2024.

COPYRIGHT © 2024 by the Society of Nuclear Medicine and Molecular Imaging.

may be slow (and therapeutic) in the cortex but fast (and addictive) in the striatum (5,6). These are just a few examples to motivate the use of PET to study the nonsteady state of the brain.

Thus, we can think about 2 classes of experimental goals: to probe the steady state unobtrusively, or to perturb it intentionally and measure its response. If the temporal pattern of dopamine release is of interest, for example, the latter class of experiment is required and demands that the design of the experiment and the mathematic treatment of the data be approached differently from the more common scenarios in which the steady state is to be probed.

For a bolus injection of a tracer in a steady state experiment, a kinetic model containing static parameters may be all that is needed to describe the resulting dynamic data. The parameters typically describe rate constants governing the uptake and retention of the tracer. They are assumed not to change—at least for the duration of the measurement (i.e., the scan) period. When the system is at steady state, the use of a model with static parameters, also known as a time-invariant (parameter) model, is appropriate and sufficient.

On the other hand, for a bolus injection of a tracer in a non-steady state experiment (i.e., one with an intentional perturbation of the steady state), a time-invariant model may be inadequate to describe the resulting dynamic PET data. In fact, the application of a time-invariant model to data from a system not at steady state could be folly. It could lead to grossly incorrect and misleading interpretations of the data. Some possible misinterpretations of dynamic raclopride data, acquired during a dopamine-altering perturbation but subjected to analysis by a time-invariant model (and used to estimate change in BP), have been described by Yoder et al. (7). The susceptibility to misinterpretation of common forms of kinetic models used in PET has been cataloged and explained by Sullivan et al. (8).

Faced with a non-steady state system, what is the diligent PET modeler to do? Luckily, there has been sustained progress in the development of time-varying kinetic models for the purpose of characterizing dynamic PET data acquired while significant changes are occurring in brain processes (Table 2 lists some important features of the different time-variant models). In effect, these models are intended, first, to describe the underlying biology of competition for receptor binding sites between a radioligand and a neurotransmitter or administered drug and, second, to detect and extract a transient signal from the dynamic PET data arising from this competition (Fig. 1). What is more, as awareness has grown of the need for yet better-performing models and algorithms (better sensitivity, better robustness to noise), the development, refinement, and even rethinking of

the earliest incarnations of the time-variant models have accelerated. These new variations on an earlier theme have drawn on innovations in mathematics, image processing, artificial intelligence, and statistics to improve the performance of the earliest practical time-variant models introduced to describe non-steady state conditions.

This article reviews some of the history and noteworthy applications of early time-variant models and then describes and contrasts more recent innovations and their theoretic underpinnings (Table 2). We conclude with some discussion of a parallel development in Bayesian statistics that could afford synergies with time-variant models. Bayesian analysis methods offer the advantages of use of prior information, as well as the important ability to assess the posterior probability (i.e., confidence) of a given result, even at the individual-subject level.

HISTORICAL PERSPECTIVE ON THE DEVELOPMENT OF NONSTEADY MODELS IN PET

In the late 1980s and early 1990s, what were then called activation studies were exclusively the domain of PET and blood flow tracers, most commonly [^{15}O]water (9). These studies, involving tasks (control/stimulus) performed repeatedly by a subject after serial injections of the tracer, were technically difficult (the half-life of [^{15}O] is 2 min). The desired signal was a local change in blood flow. Such studies have now been almost entirely supplanted by blood oxygenation level-dependent functional MRI, which can measure a surrogate of blood flow changes with much greater spatial and temporal resolution. But PET studies of brain activation are of historical interest because they indicate that the PET imaging field, even as early as the 1980s, was concerned with transient brain responses to external stimuli.

Coupled with an interest in brain activation was a rapidly expanding library of receptor- and enzyme-specific PET tracers that were being used primarily to measure the density of targets. A prominent early target was the dopamine receptor (and its various subtypes); another was the aromatic amino acid decarboxylase, a critical enzyme in the synthesis of dopamine from L-3,4-dihydroxyphenylalanine. [^{11}C]raclopride and [^{11}C]-N-methylspiperone were two of the earliest dopamine-receptor tracers in use. Aromatic amino acid decarboxylase was successfully imaged with [^{18}F]-6-L-3,4-dihydroxyphenylalanine. In 1983, two watershed papers were published within a week of each other. One (10) reported the first dopamine receptor images in a living human brain, and the other (11) revealed the first images of aromatic amino acid decarboxylase in the same. An image from the latter was actually the cover image of the issue of *Nature* in which it appeared. Some of the earliest work to turn the images into quantitative assessments was done by Mintun et al. (12), who introduced time-invariant kinetic models based on mass balances to fit dynamic PET data. The group at Brookhaven (13) also introduced some of the earliest time-invariant kinetic models to quantify uptake and retention of ^{18}F -labeled tracers for the dopamine receptor—spiperone, benperidol, and haloperidol—all based on neuroleptic drugs.

In a landmark study, Koeppe et al. (14) demonstrated the feasibility of using [^{11}C]raclopride PET and a time-invariant model to measure elevated dopamine levels in subjects playing a video game (14). The investigators assumed their subjects could maintain an elevated but steady dopamine state for the duration of a 50-min PET activation scan and performed a groupwise comparison with control scans performed on the same subjects without the rewarding stimulus. Under this assumption, BP is an appropriate

NOTEWORTHY

- If the available number of binding sites for a PET tracer changes within the time frame of a PET scan, steady-state models (with time-invariant parameters) may be inadequate to describe time-activity curves derived from the PET data.
- There is a long history (at least 3 distinct generations) of kinetic models that have been introduced in the PET-modeling field that accommodate transient (time-varying) effects in dynamic PET data.
- As models and methods continue to improve, the ability to detect brief transient effects (the sensitivity) improves. With these improvements, our ability to test yet more subtle hypotheses about neurotransmitter action and other brief neurochemical events improves.

TABLE 1
Definitions of Variables and Terms

Term	Unit	Description
B_{\max}	nM	Receptor density
k_{on}	(1/nM)(1/min)	Association rate constant*
k_{off}	1/min	Dissociation rate constant*
$K_D = k_{\text{off}}/k_{\text{on}}$	nM	Equilibrium dissociation constant (1/affinity)
$C_T(t)$	nM	Concentration of tracer in tissue
$C_P(t)$	nM	Concentration of tracer in plasma
V_T	mL (plasma)/mL (tissue)	Volume of distribution = C_T/C_P (at steady state)
$BP = B_{\max}/K_D$	Unitless	Binding potential (also nondisplaceable BP [†])
ΔBP	Unitless	Fractional changes in binding potential = (BP _{condition 1} - BP _{condition 2})/BP _{condition 1}
K_1	1/min [‡]	Influx rate constant from blood to tissue*
k_2	1/min	Efflux rate constant from tissue to blood*
k_3	1/min	Binding of ligand to receptor
k_4	1/min	Dissociation of ligand from receptor
R_1	Unitless	Relative influx ($K_1 \text{ tissue}/K_1 \text{ reference}$)
$B(t)$	nM	Concentration in bound compartment
$F(t)$	nM	Concentration in free compartment
γ	1/min	Magnitude of transient change in neurotransmitter level (21,42)
$h(t)$	Unitless	Activation profile (typically pure exponential or Gamma-variate)
T	Min	Take-off time of neurotransmitter response (21)
τ	1/min	Control rate at which activation effects are attenuated (21)
$k_{2a}(t) = k_{2a} + \gamma \times h(t)$	1/min	Apparent efflux rate constant accounting for time dependency
$k_{2a} = k_2/(1 + \text{nondisplaceable BP})$	1/min	Apparent efflux rate constant given 1-compartment representation (21,42)
γ/k_{2a}	Unitless	Normalized magnitude of neurotransmitter change
Basal	nM	Neurotransmitter concentration at steady state
G	nM	Amplitude of fluctuation in neurotransmitter
$(t - t_D)^\alpha \times (\exp(\beta(t - t_D)))$	nM	Temporal pattern of fluctuation in neurotransmitter
t_D	Min	Take-off time of neurotransmitter response
t_P	Min	Peak time of neurotransmitter response (42)
α	Unitless	Steepness and duration of function's ascent after take-off (t_D) of neurotransmitter response (37,41) or sharpness of neurotransmitter response as defined by Normandin et al. (42) (depends on Gamma-variate equation used)
β	—	Two meanings of β : rapidity with which Gamma-variate curve returns to basal state (37,41) or regression weight in units of % signal change in residual space detection equation (61)
RSD	—	Residual space detection
FPR	—	False-positive rate
p^{eff}	—	Effective number of parameters (it can be fractional number) applied to statistical metrics with lp-ntPET model (54)
$P(X Y)$	—	Conditional probability of outcome X given Y is true
Y_{obs}	—	Observed PET data (typically time–activity-curve)
θ_m	—	Vector of model parameters
$P(Y_{\text{obs}} \theta_m)$	—	Likelihood function, that is, probability of observed PET measurements Y_{obs} given model parameters θ_m
$P(Y_{\text{obs}})$	—	Marginalized likelihood
$P(\theta_m)$	—	Prior probability of model parameters θ_m
$P(\theta_m Y_{\text{obs}})$	—	Posterior probability of model parameters θ_m given PET measurements Y_{obs}

*ref and DA added as superscript refer to reference tissue and dopamine, respectively.

[†]Refer to Innis et al. (74).

[‡][mL (plasma)/mL (tissue)]/min.

TABLE 2
Characteristics of Time-Varying Models

PET model or implementation	Description/innovation	Assumptions	Limitations	Application
Extensions of 2-tissue-compartment neurotransmitter model (16,17)	First generation: shift in perspective; explicit aim of detecting dopamine fluctuations	Transient dopamine elevation modeled as square wave	Is impractical because of computationally demanding nonlinear estimation of many parameters	
LSRRM (21)	First generation: extended version of MRTM, a linearization of simplified reference tissue model; accommodates non-steady state conditions; includes time-variant efflux, presumed to be due to increased competition by neurotransmitter with tracer	Temporal pattern of dopamine release fixed in shape: pure exponentials	Cannot represent the dopamine function as a fixed shape function, $h(t)$, if the hypothesis is about the shape of the dopamine function	(25–33)
ntPET (37)	First generation: description of competition between neurotransmitter and labeled tracer; set of 3 explicit mass balance equations coupled by bimolecular binding term made up of product of instantaneous concentration of available receptor sites and free competitor	Use of reference tissue	Is not linearizable because of nonlinear binding term; has 12 parameters, some of which were not identifiable; estimates multiple possible dopamine curves that could fit each dataset equally well	(38,41,42)
Nonparametric ntPET (39)	Second generation: nonparametric singular value decomposition of PET time-activity curves; data-based method does not assume shape of dopamine curve		Requires training set	(40,43)
lp-ntPET (42)	Second generation: linearized version of ntPET model; same operational equation as Equation 1 (LSRRM) except that $h(t)$ is allowed to vary in shape; multiple choices of $h(t)$ are represented as basis functions	Library of basis functions created with discretized parameters that span realistic range	Possibly overfits noise; has possible overly conservative model selection criteria	(42,47,48,50,52)
Denosing as preprocessing (55)	Third generation: controls FPR—feed-forward neural network that was trained to denoise PET time-activity curves by predicting noiseless time-activity curve		Requires training set	
Corrected model selection (54)	Third generation: controls FPR—adaptive model comparison metrics that control FPR regardless of number of basis functions used		Requires simulation of null data for every application	(33,56,72)
Direct reconstruction (57)	Third generation: controls FPR—noise is well known (Poisson) in sinogram domain; consequence is reduction of FPR		Assumes same kinetic model at all locations	
Machine learning (58)	Third generation: controls FPR—preselects voxels most likely to contain activation		Requires training set	
Monte Carlo modeling/ F -statistic correction (59)	Third generation: improves sensitivity—corrects F distribution for errors introduced by partial volume		Needs to simulate null and activated data for every application	

(continued)

TABLE 2
Characteristics of Time-Varying Models (cont.)

PET model or implementation	Description/innovation	Assumptions	Limitations	Application
Personalized neural nets (60)	Third generation: improves sensitivity—differentiates noisy time–activity curves with and without effect of dopamine release; outperformed <i>F</i> -test in identified real activations		Needs to simulate null and activated data for every application	
Residual space analysis (61)	Third generation: improves sensitivity—converts time–activity curves into residual curves, defining canonic baseline curve (no effect of activation) and subtracting it from each voxel time–activity curve		Requires sufficient nonactivated voxels to serve as baseline	
b-ntPET (64)	Beyond third generation: Bayesian method, uses Markov chain Monte Carlo sampling; produces posterior distribution of model parameters	Validity of prior distributions	Requires analytic expression of likelihood function; convergence is slow; not easily extended to voxels	(64)
PET-ABC (65,66)	Beyond third generation: simplifies Bayesian computation; is extensible to voxel level; produces probability-of-activation maps for individuals	Validity of prior distributions	Generates approximate posterior distribution	(56,66,67)

outcome measure of receptor availability. But what if the assumption is incorrect?

That any of these ligands—unlike [¹⁸F]-FDG—might be displaceable by an endogenous ligand presented both a concern and an opportunity. To address the concern, Logan et al. (15) introduced a more elaborate compartmental model than in earlier papers. It described the kinetics of both the tracer raclopride and the endogenous competitor (dopamine). They did so to assess and minimize the sensitivity of estimates of BP or V_T to unintended fluctuations in endogenous dopamine. Specifically, they showed that these parameters were underestimated in the presence of a hypothesized dopamine perturbation and that the greater the amplitude or duration of the perturbation, the greater the underestimation. Their underlying goal, however, as demonstrated via simulations, was to show that the sensitivity of estimated BP to dopamine fluctuations was low and therefore manageable. By contrast, the group of Morris and Fisher at Massachusetts General Hospital (16,17) introduced a compartmental model with the opposite concern. That is, they wanted to explore and optimize a scanning protocol that would maximize the sensitivity of the PET signal to dopamine fluctuations with the explicit aim of detecting these endogenous indicators of brain activation. Their rather simple simulations (transient dopamine elevation was modeled as a square wave) suggested that a short time delay in the onset of a dopamine rise after a bolus tracer injection could maximize the dopamine effect on the measured PET data. This work represented the start of an important shift in perspective—away from steady state parameters (e.g., BP and V_T) and toward perturbations of the steady state and the parameters that characterize them. At about the same time, the Hammersmith group was presenting a

modification of the 1-compartment model that included a time-varying component of *k*₂, the efflux constant, to detect a transient response to an infusion of midazolam (18). This group chose a fixed exponential to model the effect of displacement.

The sensitivity of steady state parameters to experimental conditions (specifically, those that cause fluctuations in dopamine) was further characterized mathematically by Endres and Carson (19). Their primary finding was that the estimated change in V_T (ΔV_T) of a tracer (caused by the change in an endogenous competitor) can be formulated as a weighted average of the instantaneous V_T over the course of the scan. And, critically, the weighting function depends on the instantaneous concentrations of both free tracer and endogenous ligand in the tissue. Thus, anything that alters the free tracer concentration or the endogenous ligand (e.g., dopamine) even for a short time affects the estimate of ΔV_T . So, timing matters. A follow-up simulation study by Morris and Yoder (20) leveraged the Endres and Carson (19) derivation of ΔV_T in the presence of a time-variant endogenous competitor to demonstrate that the rate constant of dissociation of the tracer from the receptor (which does not always follow the affinity) was the most important characteristic in selecting the best tracer to maximize the detectability of transient changes in endogenous ligand.

METHODS OF DETECTING DOPAMINE TRANSIENTS IN DYNAMIC PET DATA

First-Generation Innovations

Once the limitations of conventional kinetic models with time-invariant parameters were recognized, a series of extensions to the standard 2-compartment model was proposed and developed (16,17).

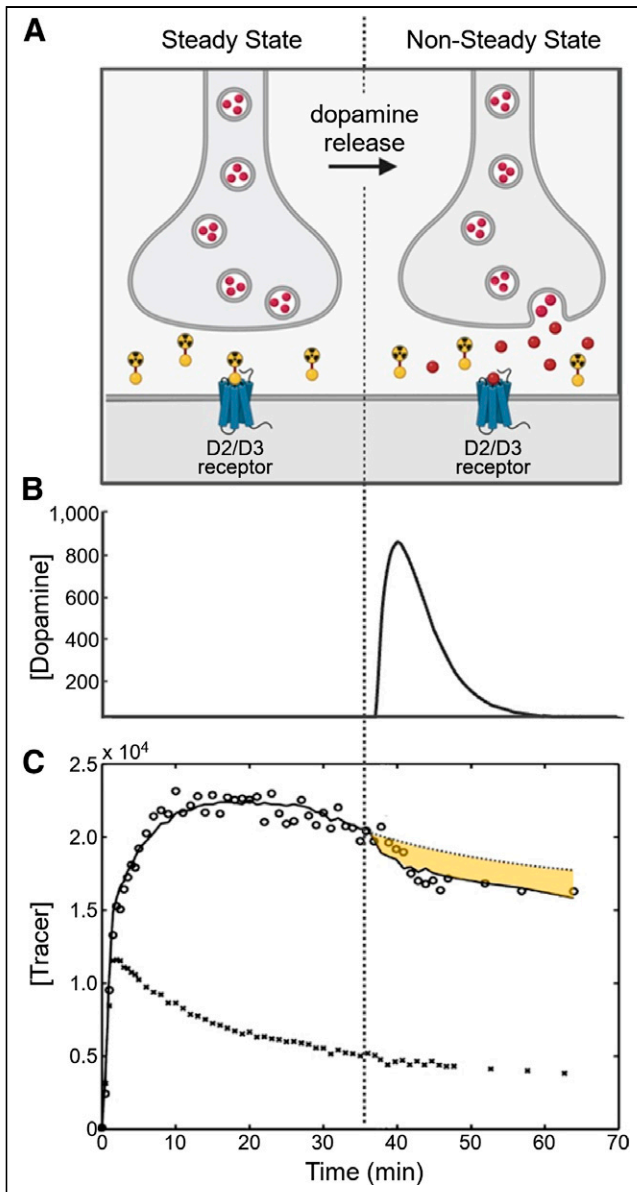


FIGURE 1. Schematic of transient dopamine release and effect on dynamic PET curve. (A) Under steady-state conditions (left half of panel), number of D₂/D₃ binding sites available for binding are approximately constant. After external stimulus (right half of panel), neurotransmitter dopamine is released from synaptic vesicles into synaptic cleft. (B) Rise in dopamine in synapse (right half of panel) causes non-steady-state scenario, reflected by transient change in dopamine signal and fewer available binding sites. (C) Transient drop in available binding sites (right half of panel) causes deflection in PET time-activity curve from steady-state trajectory (dotted curve) in regions of specific binding (open circles) but not in regions lacking dopamine receptors, such as cerebellum (filled symbols). (A created using BioRender.com; C reprinted with permission of (27).)

Some extensions were computationally demanding (they required nonlinear estimation of many parameters) and were thus impractical for widespread use. The earliest practical solution to the presence of transient effects in PET data was addressed by the introduction of the linear simplified reference region model (LSRRM) by Alpert et al. (21). In this review, we refer to LSRRM as a first-generation nonsteady kinetic modeling innovation. In effect, it incorporates

nonsteady behavior into the time-variant dissociation rate constant of a 1-compartment model. The model allows for the identification of region- or voxel-level effects of neurotransmitter (specifically, dopamine) release on tracer uptake and efflux immediately after a drug or behavioral challenge. LSRRM derives its strength and practicality from its simplicity. First, it is a reference region model. The input function can be derived from the image data. Second, it is an integral equation. Its parameters of interest can be estimated via linear regression. It is useful for detecting neurotransmitter release if the release begins at a known time, for example, after administration of a fast-acting intravenous drug. But it achieves its simplicity by assuming an instantaneous effect of a stimulus on neurotransmitter concentration and a fixed rate constant for return of neurotransmitter level to baseline. Thus, it may not be well suited to characterize a slow response or one that occurs at an arbitrary time, for example, after a behavioral task or delayed reward. In every experiment, one must keep in mind the end goal. If detection of an event is primary, then a biologically simplistic model may yet be preferred over greater biologic accuracy, provided the simple model is the most sensitive.

Strengths. LSRRM, introduced in 2003 (21), was derived as an extension of the simplified reference tissue model (22,23). But because LSRRM is formulated as an integral equation, it is convenient to think of it as an extended version of the popular time-invariant model, namely, the multilinear reference tissue model (MRTM) (24). The simplified reference tissue model is based on a 1-compartment model. In turn, MRTM is a linearization of the 1-compartment model. It is routinely applied to data, via multilinear regression, to estimate the static parameter nondisplaceable BP (the level of available receptors) assuming steady state conditions. By contrast, LSRRM (Eq. 1) can accommodate non-steady state conditions. LSRRM contains a term (at far right in Eq. 1) that acts as a time-variant efflux, presumed due to increased competition by dopamine (or other endogenous ligands) with the tracer (e.g., [¹¹C]raclopride) at the receptor site.

$$C_T(t) = R_1 C_R(t) + k_2 \int_0^t C_R(u) du - k_{2a} \int_0^t C_T(u) du - \gamma \int_0^t C_T(u) h(u) du, \quad \text{Eq. 1}$$

$$\text{where, } h(t) = \begin{cases} 0, & t < T \\ e^{-\tau(t-T)}, & t \geq T \end{cases} \quad \text{Eq. 2}$$

is the dopamine curve over time, $C_T(t)$ is the tissue curve, and $C_R(t)$ is the reference tissue curve. γ is the magnitude of dopamine response. $C_T(t)$ and $C_R(t)$ are derived from target and reference regions, respectively, in the PET images. In the original publication by Alpert et al. (21), LSRRM was used to fit PET time-activity curves at the voxel level acquired during a planned motor task (Fig. 1C).

LSRRM has subsequently been used by many to detect dopamine activation in response to a behavioral task (25–32). Zakiniaciz et al. (33) used it recently to demonstrate that spatial patterns of cigarette-induced dopamine activation during smoking are altered by nicotine replacement therapy (i.e., the nicotine patch). Supplemental Figure 1 (supplemental materials are available at <http://jnm.snmjournals.org>) shows images of the change (both positive and negative) in the magnitude of dopamine release, γ/k_{2a} , derived from the application of LSRRM at the voxel level to dynamic [¹¹C]raclopride PET images of smokers smoking in the scanner under nicotine replacement therapy and placebo. The primary concern of the investigators in the study was to identify spatial patterns

rather than timing, that is, presence and location of activation. Their findings were made all the more interesting by the observation that the patterns of dopamine activation were related to known markers of smoking treatment outcome, namely, severity of dependence, Fagerstrom test for cigarette dependence, and nicotine-to-metabolism ratio. The subtle differences in dopamine release under placebo and patch are unlikely to have been observed using conventional time-invariant models. But what other support can we find for the use of γ over change in BP as an endpoint for detecting dopamine change?

A beautiful demonstration of the added power of the first-generation model, LSRRM, over conventional time-invariant kinetic models is available thanks to a natural experiment in the PET literature. Two prestigious research groups each conducted PET imaging experiments applying the same stress task (the Montreal Imaging Stress Task, which combines mental arithmetic by the subject with negative feedback by the investigator (34)) for a limited time in the scanner during the scan session with the intent of stimulating dopamine release but used different analysis methods (29,35). The cohorts were similar. One group of investigators (35) estimated change in BP, based on conventional time-invariant models, whereas the other (29) estimated the amplitude of the transient dopamine component, γ , using LSRRM. Supplemental Figure 2 shows the uncorrected t score maps for the respective analyses. The first-generation analysis (with a non-steady state term for dopamine) detected a more widespread effect than the conventional one. A comparison of the 2 analyses (including differences in search volume) is detailed in a review by Liu et al. (36). LSRRM and γ are better suited than conventional time-invariant models and change in BP for detecting short-lived dopamine responses to stimuli presented during the scan.

Limitations. The main limitation of the first-generation model, LSRRM, is that the temporal pattern of dopamine release is fixed in shape. $h(t)$ (Eq. 2) is prescribed as a decaying exponential with instantaneous take-off at the presumed time of activation and a fixed decay rate of dopamine back to baseline. If one has a hypothesis about the time course of dopamine release (e.g., a drug or condition is affecting the particular shape of the dopamine response to a stimulus), then a model with a predetermined shape, $h(t)$, cannot be used to test it.

In response to perceived limitations of LSRRM, Morris et al. (37) introduced neurotransmitter PET (ntPET), diagrammed in Figures 2A and 2B (37). ntPET was originally developed to describe dopamine responses to drugs, such as ethanol (28) or methamphetamine (29), (both of which increase dopamine release directly or indirectly) in animals. The difficulty of taking blood samples in rodents, however, demanded the development of a reference region model (i.e., a model whose plasma input function is described in terms of an image-derived reference region curve; Fig. 2B). For flexibility, ntPET was configured as a set of 3 explicit mass balance equations (Eqs. 3–7) coupled by a bimolecular (and thus nonlinear) binding term made up of the product of the instantaneous concentration of available receptor sites (in brackets) and the free competitor (either dopamine or tracer). This term describes the critical phenomenon being imaged, namely,

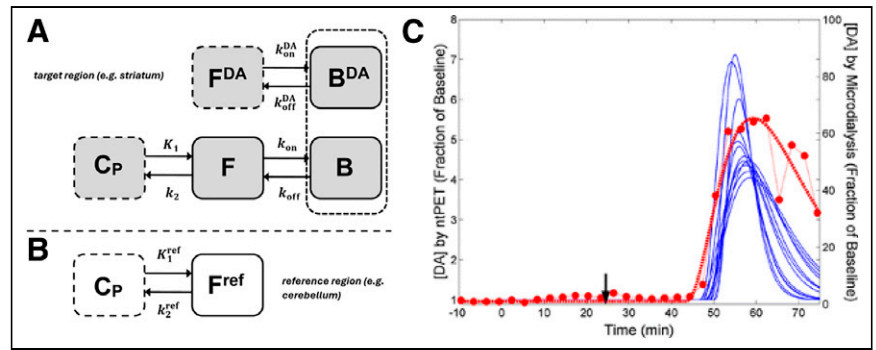


FIGURE 2. Graphical representation of ntPET model and estimated dopamine curves with ntPET model compared with microdialysis. (A) Two-species model for tracer uptake from plasma to free and bound states in presence of time-varying dopamine (in free and bound states). Note absence of supply of dopamine from plasma to free compartment (as in case of tracer) because dopamine does not originate in plasma. It is injected into synapse by presynaptic neuron. Hence, dopamine generation can be modeled as originating within free dopamine compartment. (B) One-compartment model description of reference region lacking dopamine receptors. (Reprinted with permission of (37).) (C) Family of dopamine curves resulting from multiple best fits to PET data (blue) compared with smooth function fit directly to microdialysis data (red curve through red circles). There is some ambiguity in magnitude of estimated dopamine curves, but temporal agreement between PET estimates and microdialysis is quite good. DA = dopamine. (Reprinted with permission of (38).)

competition between the neurotransmitter dopamine and the labeled tracer. Unfortunately, the use of a nonlinear binding term meant the model was not linearizable à la MRTM (24) or LSRRM (21).

The following equations describe the ntPET model:

$$\frac{dF(t)}{dt} = K_1 C_p(t) - k_2 F(t) - k_{on}[B_{max} - B(t) - B^{DA}(t)]F(t) + k_{off}B(t) \quad \text{Eq. 3}$$

$$\frac{dB(t)}{dt} = k_{on}[B_{max} - B(t) - B^{DA}(t)]F(t) - k_{off}B(t) \quad \text{Eq. 4}$$

$$\frac{dB^{DA}(t)}{dt} = k_{on}^{DA}[B_{max} - B(t) - B^{DA}(t)]F^{DA}(t) - k_{off}^{DA}B^{DA}(t) \quad \text{Eq. 5}$$

$$F^{DA}(t) = \text{basal} + G \times [t - t_D]^\alpha \exp(-\beta[t - t_D]) \quad \text{Eq. 6}$$

$$C_p(t) = \frac{1}{K_1^{ref}} \left[\frac{dF^{ref}(t)}{dt} + k_2^{ref} F^{ref}(t) \right]. \quad \text{Eq. 7}$$

In practice, the ntPET model was unwieldy. It contained 12 parameters, some of which were not identifiable, resulting in estimation of multiple possible dopamine curves that could fit each dataset equally well. Reflecting the nonidentifiability, a collection of multiple possible estimated free dopamine curves, $F^{DA}(t)$, in the striatum from images of a rat administered methamphetamine is shown in Figure 2C. The curves are nonetheless consistent and plausible, as demonstrated (Fig. 2C) by comparison with simultaneous microdialysis measurements of striatal dopamine (from Morris et al. (38)). With regard to practicality, nonlinear terms in the model required iterative numeric solution and nonlinear fitting. The computation time to solve the ntPET equations was long.

Second-Generation Innovations

Strengths. In efforts to make the estimation of dopamine transients more practical, Constantinescu et al. (39,40) and Norman-din et al. (41,42) took complementary mathematic approaches and introduced a nonparametric ntPET model and a linear parametric ntPET model (lp-ntPET), respectively. The former was based on a singular value decomposition of the PET time-activity curves. In

2010, the singular value decomposition approach was used to create parametric images of the timing of a dopamine response to finger tapping (43). Nonparametric ntPET was an early attempt at a data-based method of analysis of dynamic PET data. The need to train the nonparametric ntPET model on simulated data anticipated the use of the machine learning methods discussed below.

Although nonparametric ntPET was based on a signal-processing approach to the problem, lp-ntPET resulted from a modeling approach. As we show below, later methods have merged signal processing and modeling to great effect. lp-ntPET is a linearized version of the ntPET model. It is structurally similar to Equation 1 (LSRRM) except that $h(t)$ is allowed to vary in shape. For lp-ntPET, $h(t)$ takes a more complicated but also better-behaved form that facilitates estimation of an explicit peak time term, t_p (44),

$$h_i(t) = \left(\frac{t - t_D}{t_p - t_D} \right)^\alpha \exp \left(\alpha \left[1 - \frac{t - t_D}{t_p - t_D} \right] \right) u(t - t_D). \quad \text{Eq. 8}$$

The combination of Equations 1 and 8 would still require nonlinear fitting because of the unknown parameters of $h(t)$ were it not for the key innovation of Normandin et al. (42) to implement lp-ntPET using preselected basis functions (22,45). Each basis function corresponds to a preselected combination of α , t_p , and t_D to represent a unique $h(t)$. Thus, in practice, lp-ntPET is fit to data through a series of linear fittings to $C_T(t)$, one for each of the predetermined basis functions. There are only 4 linear parameters to be estimated: R_1 , k_2 , k_{2a} , and γ . The computation time is greatly reduced compared with ntPET, and fitting data at every voxel to produce parametric images becomes more tractable.

Because lp-ntPET allows for different possible shapes of the dopamine curve in time, the group at Yale used it to test the hypothesis that there are distinct areas of the ventral striatum in which male and female smokers respond at different speeds to smoking cigarettes (46). In their analysis of a cohort of 8 male and 8 female smokers smoking in the scanner (47), they were able to identify an area of dorsal putamen in which women responded with faster dopamine release (shorter rise time) than men to smoking a cigarette. Supplemental Figure 3 (left) shows this result as an image, and Supplemental Figure 3 (right) shows the temporal differences between the sexes as mean time curves for the identified cluster of activation. The mean curves include the responses of some subjects in each cohort whose dopamine response was estimated to begin before the start of smoking. Such responses, if confirmed, could be interpreted as anticipation of reward.

lp-ntPET analysis has been applied to other forms of drug administration in the scanner because, like cigarette smoking, they must also be described by a model that accommodates transient responses. Calakos et al. (48) applied lp-ntPET analysis to cannabis smoking in the scanner and detected consistent areas of activation in the ventral striatum. Supplemental Figure 4 shows the location of a cluster of activation in the right ventral striatum. The timing of the response was preliminarily found to be related to the level of δ^9 -

tetrahydrocannabinol in the plasma before scanning (i.e., the level due to habitual drug use).

The second-generation model, lp-ntPET, has also found applications beyond human imaging. Kyme et al. have perfected open-field PET imaging of freely moving awake rats (49). This capability makes possible experiments to examine the brains of awake animals responding to drugs and other stimuli without the confounds of anesthesia. In this study, lp-ntPET was used to estimate the temporal pattern of [^{11}C]raclopride displacement by a pharmacologic dose of unlabeled raclopride in awake rats (Fig. 3) (49). The responses of 4 rats were consistent in time and magnitude (Fig. 3D). When the limits of first-generation methods are considered, the gradually peaking shape of the estimated dopamine curve (Fig. 3D) is not consistent with an instantaneous peak and single exponential decay (as imposed on the response shape by LSRRM).

The lp-ntPET model was initially applied at the region-of-interest level. But its great promise is at the voxel level to identify and characterize localized brain clusters of unique kinetics because of unique temporal effects of transient neurotransmitter activation. As mentioned above, fitting models with nonlinear terms is generally iterative. Thus, applying models on the voxel level can be computationally demanding. Furthermore, voxel-level PET time-activity curves are much noisier than region-of-interest-level curves. To address these challenges, lp-ntPET was implemented as a 4-step pipeline (first introduced by Kim et al. (50)).

The first step is preprocessing. Highly constrained backprojection filtering applied to the dynamic PET images is a method of spatial filtering that has the desirable property of preserving temporal edges without compromising spatial resolution (51). The contribution of highly constrained backprojection to the overall sensitivity of the pipeline has been isolated via the analysis of simulations by Wang et al. (52).

The second step is selection of basis functions. The lp-ntPET model is discretized by preselecting a library of $h(t)$ curves. Each

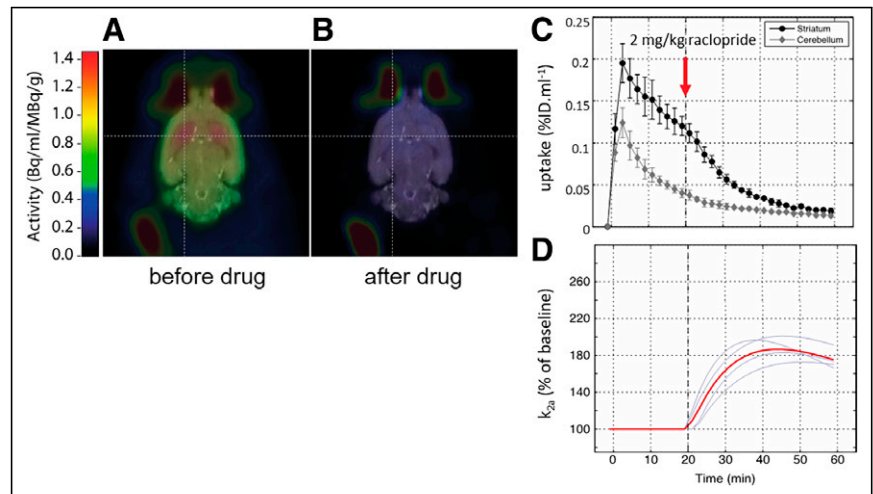


FIGURE 3. Application of second-generation model, lp-ntPET, to awake rats. (A) Motion-corrected PET data showing integrated [^{11}C]raclopride distribution in brain of representative freely moving rat over first 20 min of study (before administration of unlabeled raclopride), superimposed on spatially registered MRI brain template. (B) Reconstructed PET image integrated over last 20 min of study, after administration of unlabeled raclopride. (C) PET time-activity curves averaged across 4 animals (mean \pm SD) for striatal and cerebellar regions of interest. (D) Four individual (gray) and mean (red) estimated replacement of [^{11}C]raclopride by (unlabeled) raclopride (k_{2a}) curves obtained from kinetic modeling of dynamic PET data in C using lp-ntPET. %ID = percentage injected dose. (Reprinted with permission of (49).)

basis function in the library is a curve resulting from a fixed set of parameters t_p , t_D , and α . For each given basis function, fitting the model to the data is a linear problem and so proceeds almost instantaneously. For a limited number of basis functions, the lp-ntPET model can be applied at each voxel quickly.

The third step is model selection. To determine whether transmitter activation is significant, each voxel-level time–activity curve is fit with MRTM and lp-ntPET. The activation is deemed significant (and a nonzero γ value is retained) if the lp-ntPET fit is statistically better than the MRTM fit based on standard model comparison metrics such as the F test (or the corrected Akaike information criterion or corrected Bayesian information criterion) (42,50,53,54).

The fourth step is application of a cluster-size threshold. To counteract the false positives that occur whenever multiple comparisons are performed (at large numbers of voxels), a cluster-size threshold is applied to retain only those clusters of activated voxels that are large enough to not have occurred by chance in null data (i.e., dynamic PET data in the absence of any neurotransmitter activation).

Limitations. The main limitations of the second-generation model, lp-ntPET, as with all detection methods, are too many false positives or too many false negatives. Understanding what causes what leads directly to improvements. False positives are generally the result of oversensitivity of lp-ntPET (i.e., overfitting) to noise, the magnitude of which rivals, in some cases, that of the signal of interest (i.e., the dopamine effect). False negatives are generally attributable to overly conservative rejection of activated voxels by model selection criteria or cluster-size thresholds intended to control false positives at the voxel or image level, respectively.

Third-Generation Innovations

Strengths—Controlling False Positives. To control the false-positive rate (FPR, defined in Table 2), investigators have worked to better model the noise or to reduce it. Reduction of noise by a naïve method (i.e., not accounting for the expected time–activity curve shape), such as gaussian smoothing in time, runs the considerable risk of smoothing out any abrupt effect of neurotransmitter release. Angelis et al. (55) introduced a feed-forward neural network that was trained to denoise the PET time–activity curves by predicting the noiseless time–activity curve. The method was successfully trained on 40 million simulated time–activity curves that contained or did not contain the effect of dopamine release caused by an idealized stimulus starting at 20 min into a dynamic raclopride scan. The true response to the stimulus (portrayed in red in Supplemental Fig. 5) persists for about 20 min. The performance of neural network denoising exceeded the performance of second-generation denoising with highly constrained backprojection. The comparison of the denoised images and the resultant fits of lp-ntPET to realistic simulated rat data containing a dopamine perturbation is shown in Supplemental Figure 5.

In third-generation work, Liu and Morris (54) discovered an unwanted dependence of FPR on the number of basis

functions in the lp-ntPET implementation. This is because a limited basis created from triplets of discretized parameters, t_p , t_D , and α , cannot span all of parameter space. Consequently, the degrees of freedom (number of parameters in a model subtracted from number of data points in time–activity curve) used by a model-comparison metric (e.g., the F statistic) to determine the best-fit model is too strict and must be adjusted. By introducing the concept of effective number of parameters (p^{eff}), Liu and Morris were able to control the FPR regardless of the number of basis functions used. Looking across the rows in Figure 4A, one observes that the correction for p^{eff} applied to the model comparison metric (the Akaike information criterion) controls the FPR across a wide range of basis function library sizes (8–60 basis functions).

As a further illustration of the potential impact of the correction for p^{eff} , a dataset from Zakiniaez et al. (33) was recently analyzed with LSRRM, lp-ntPET, and lp-ntPET with the Bayesian information criterion corrected for the p^{eff} . The preliminary result of this comparison of methods is shown in Figure 4B (56). Looking at a single human dataset, we cannot assess the accuracy of the analysis. But the progressively larger areas of detected activation support the claim that sensitivity to transient dopamine activation is improved from first- to second- to third-generation innovations. We recognize that sensitivity is not the same as accuracy. Whether the detection of additional activation is correct (more true positives) or not (more false positives) can be determined only through the analysis of simulated data for which ground truth is known.

Angelis et al. (57) also incorporated lp-ntPET into direct reconstruction. Because direct reconstruction fits the data in the sinogram domain, where the noise model is better characterized than in the image domain, the effect of noise on model fitting is minimized. This, in turn, has the result of reducing the FPR of lp-ntPET.

Fuller et al. (58) used various machine learning algorithms both to denoise and to identify time–activity curves that were activated (containing a dopamine transient) on the basis of training with

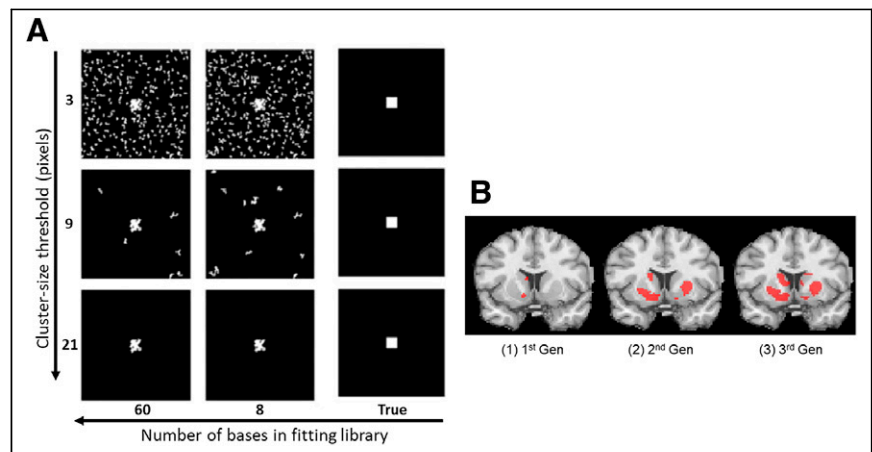


FIGURE 4. (A) Performance of third-generation innovation: demonstration of correction for p^{eff} in model implementation. Number of bases declines to right. True image is in far right column. Cluster-size threshold is increased down columns. White indicates pixel for which full model (lp-ntPET) is found to be superior to restricted model (MRTM). Visible in center of phantom is 10×10 pixel positive region; rest of phantom is null. All white voxels in null region are false positives. FPR decreases with increased cluster-size threshold but remains stable across number of bases. (Reprinted from (54).) (B) Performance of first, second, and third generations (Reprinted from (56).) Shown is activation (red) detected at voxel level in dynamic raclopride images of cigarette smoking in scanner by first generation (LSRRM), second generation (lp-ntPET), and third generation (lp-ntPET with adaptive model comparison (54)); method's performance is described in A. Gen = generation.

256,000 noisy simulations of activated and nonactivated (dopamine transient absent) time–activity curves. This approach aimed to reduce the overfitting of lp-ntPET to noise. The incorporation of machine learning algorithms far outperformed the second-generation lp-ntPET pipeline for specificity (true negatives/[true negatives + false positives]) by reducing false positives. The superior performances of 4 different machine learning algorithms as compared with lp-ntPET are demonstrated by the authors for a wide range of noise levels and activation levels (at strict and relaxed thresholds on γ). See Figure 5 in original paper (58).

Strengths—Controlling False Negatives. The second major thrust of third-generation innovations has been to improve sensitivity, that is, to reduce the overexclusion of bona fide instances of activation (yielding a high false-negative rate). Investigators have introduced to the original second-generation pipeline various creative improvements that substitute new procedures for the model comparison and the cluster-size threshold steps. The second-generation steps were intended to identify activation and correct for multiple comparisons. But if either of these steps is too strict or invalid, it can diminish the overall sensitivity of the pipeline.

One approach has been to correct invalid assumptions that are not strictly satisfied regarding noise and parameter distributions that underlie the second-generation model selection step. Bevington et al. (59) have argued persuasively that partial-volume error (spill-in from surrounding areas not containing activation) skews the shape of time–activity curves at the periphery of clusters of activation. The altered shape leads to underestimates of γ and alters the resulting F values calculated from the fits of MRTM and lp-ntPET. In turn, these calculated F values are improperly distributed. They no longer adhere to a true F distribution. This calls into question the use of the F statistic as an indicator of best fit by lp-ntPET over MRTM and, hence, activation. Bevington et al. (59) proposed a method for finding the underlying F distribution in the presence of underestimation and then restoring the voxels that would otherwise have been rejected. The need for reassignment of F values on the F distribution is illustrated in Figure 5A. The improved recovery of activation clusters (missed by the

second-generation method) in the striatum of a human volunteer performing a gambling task is shown in Figure 5B.

A second approach to FNR has been to replace the model selection step with a neural network. Klyuzhin et al. (60) trained 4 different architectures of neural networks to differentiate noisy time–activity curves with and without the effect of dopamine release. The 2 most sensitive architectures turned out to be a dense neural net with 3 hidden layers and a convolutional neural net with 3 convolutional layers. The dense and convolutional neural nets were both trained on 100,000 noisy baseline time–activity curves and 100,000 noisy time–activity curves containing transient dopamine release. Training was performed for 300 epochs. These time–activity curves were personalized, that is, simulated to resemble [^{11}C]raclopride PET data obtained in a human subject performing a gambling task at 36 min into a 75-min scan session. The dense and convolutional neural nets both outperformed the F test in identifying activation. Supplemental Figure 6 shows the voxels that are identified as positive by the 3 methods in 2 different digital phantoms.

Bevington et al. (61) took another approach to the model selection step. They merged a data-driven approach with modeling of a step function—reminiscent of functional MRI analysis—to replace the model selection step. The investigators introduced what they called residual space analysis. By defining a canonic baseline curve (containing no effect of activation) and subtracting it from each voxel time–activity curve, they converted time–activity curves into residual curves. These residual curves were fitted to a simple model made up of a step function convolved with a smoothing function. The estimated magnitude of the step is tested for significance. The fitted residual curve and the resulting improved sensitivity are demonstrated in Figure 6. It is interesting to note that Morris et al. (17) observed that transient activation was identifiable from unique characteristics in what they called the normalized residuals (equivalent to residual space), but as is often the case, it remained for another group of investigators (61) to bring the necessary mathematical rigor to bear on the observation.

It is reasonable to assume that neural network denoising (55) could be combined with other methods. In theory, incorporating any model method into direct reconstruction (57) should improve the FPR because of the better modeling of the noisy data in sinogram space. In fact, Fuller et al. (58) showed a decrease in γ in all machine learning algorithm methods if they were incorporated into a direct reconstruction framework (Fig. 10 in the original paper (58)). Any use of direct reconstruction is, however, predicated on the availability of the list-mode data.

INTERPRETATION OF RESULTS

Once we have the results of any of the advanced methods of analysis reviewed above, we must assess whether we believe them. Said another way, what is our confidence in the results? Normandin et al. (42) grappled with this question in their lp-ntPET papers. When the data being fitted are created by simulation, there is no cost to creating and analyzing many repeated instances of the same data with different noise realizations. Normandin et al. illustrated the confidence in their results by fitting thousands of simulated

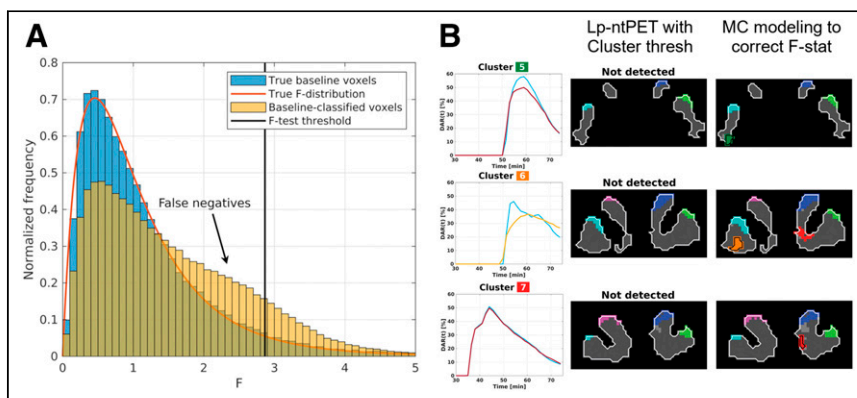


FIGURE 5. (A) Histograms (blue) of calculated F values of ground truth baseline (i.e., nonrelease) voxels from simulations. Also, histogram (yellow) of calculated F values of voxels classified (not necessarily correctly) as baseline voxels by standard model selection criterion. Yellow voxels have calculated F values that do not adhere to theoretic F distribution. These voxels should have higher F values and be captured as activated voxels. (B) Monte Carlo modeling method (third generation) performance. Shown is recovery of activation clusters in human data from subject performing gambling task. Left column shows recovered dopamine curve for clusters captured only by Monte Carlo method (color of cluster matches cluster number.) Middle column shows clusters captured in striatum by second-generation lp-ntPET algorithm. Right column shows clusters captured by Monte Carlo method. (Reprinted with permission of (59).)

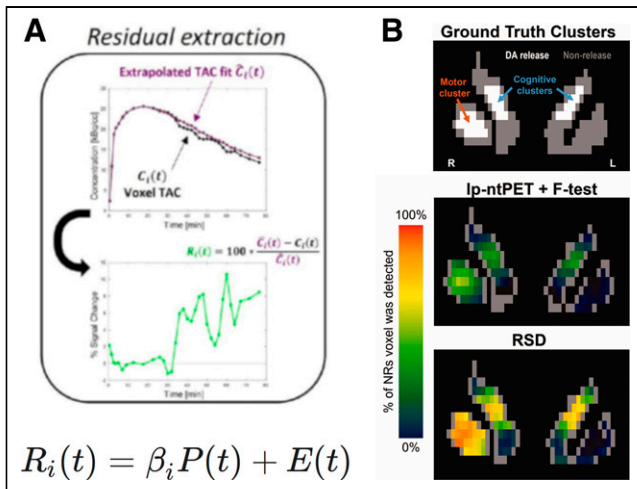


FIGURE 6. Third-generation performance. (A) Combination of time–activity curve at voxel i and canonical time–activity curve representing tracer uptake in absence of activation. Together, these two curves are converted (indicated by curved arrow) to residual space where model of $R_i(t)$ is applied. Detection becomes problem of identifying voxels with significant β_i values. (B) Bevington et al. showed their residual-space analysis to have greater detection sensitivity than lp-ntPET with F -test as model selection step. NR = number of realizations (i.e., simulations); RSD = residual-space detection; TAC = time–activity curve. (Reprinted from (67).)

datasets (same true parameters, different noise). Supplemental Figure 7 is an example. But what if we have only one dataset from a real animal or human experiment? We need a framework for assessing our confidence in the results. This leads us to the discussion of an emerging technique that could be combined with any of the variants and enhancements of the lp-ntPET model for a richer understanding of the data.

BAYESIAN STATISTICAL ANALYSIS OF NON-STEADY STATE KINETICS

Bayesian statistical approaches have been used extensively for PET image reconstruction and more recently have been extended to kinetic modeling (62,63). In frequentist statistics, probabilities are assumed to be well estimated by the frequency of random events after repeated trials. In contrast, the Bayesian statistician interprets probability conditionally, where a prior belief about the likelihood of a particular outcome is updated when new evidence becomes available, according to Bayes' rule. For example, in a PET neurotransmitter activation study, Bayes' rule (Eq. 9) can be expressed as

$$P(\theta_m | Y_{\text{obs}}) = \frac{P(Y_{\text{obs}} | \theta_m) P(\theta_m)}{P(Y_{\text{obs}})}, \quad \text{Eq. 9}$$

where Y_{obs} are the observed PET data (typically a time–activity curve), θ_m are the model parameters, $P(Y_{\text{obs}} | \theta_m)$ and $P(Y_{\text{obs}})$ are the likelihood function and the marginalized likelihood, respectively, and $P(\theta_m)$ is the prior probability of the model parameters. The model, in this scenario, would be lp-ntPET or any of the other time-variant models discussed above. Provided

we can compute the right-hand side of this expression, the term on the left-hand side, $P(\theta_m | Y_{\text{obs}})$, represents the posterior probability density function of the model parameters. In other words, we have more than just the point estimates of the model parameters, we have their probability densities as well.

Two approaches have been proposed for computing $P(\theta_m | Y_{\text{obs}})$ in the context of PET neurotransmitter activation studies: Irace et al. (64) proposed a method called Bayesian ntPET (b-ntPET), which is based on Markov chain Monte Carlo sampling. This is a random-walk algorithm that produces an unbiased estimate of the posterior distribution based on samples drawn randomly from the model parameter prior distribution and a probabilistic accept/reject criterion. Using a Bayesian framework allows the incorporation of prior knowledge of the parameters to drive the estimation. Simulation studies with null data and gradually increasing activation levels showed that the b-ntPET method reduced the FPR and that it is more robust to noise than least-squares fitting of the lp-ntPET model (Supplemental Fig. 8). In a pharmacologic challenge (with NLX-112, a serotonergic 5-hydroxytryptamine-1A agonist) in cats using the tracer $[^{18}\text{F}]\text{MPPF}$, a serotonergic 5-hydroxytryptamine-1A antagonist radioligand, the simulation results (shown in Supplemental Fig. 8) were borne out. b-ntPET detected a significant dose–response relationship due to increasing doses of NLX-112, whereas the classic fitting approach with lp-ntPET was unsuccessful (64). Similarly, b-ntPET successfully detected significant endogenous dopamine release induced by transcranial direct-current stimulation in a human $[^{11}\text{C}]\text{raclopride}$ experiment (64).

b-ntPET can be seen as a generalization of the lp-ntPET method in the sense that they both aim to optimize the likelihood function $P(Y_{\text{obs}} | \theta_m)$. Whereas lp-ntPET uses least-squares methods to do this and, in the process, directly estimates single-point parameters, b-ntPET samples the whole of the posterior probability distribution.

Although Markov chain Monte Carlo provides unbiased estimates of the model parameters and their uncertainties and has guaranteed convergence, it is computationally slow and difficult to parallelize, making voxelwise analysis impractical (63). Furthermore, Markov chain Monte Carlo requires that the likelihood function be mathematically described, but this may not be possible. Approximate Bayesian computation (ABC) addresses this issue by treating the likelihood function as the data-generating process, that is, as a model for simulating the data. Fan et al. (65,66) developed a general method named PET-ABC that adapted the ABC algorithm to kinetic modeling in PET (Fig. 7). Like Markov chain Monte Carlo,

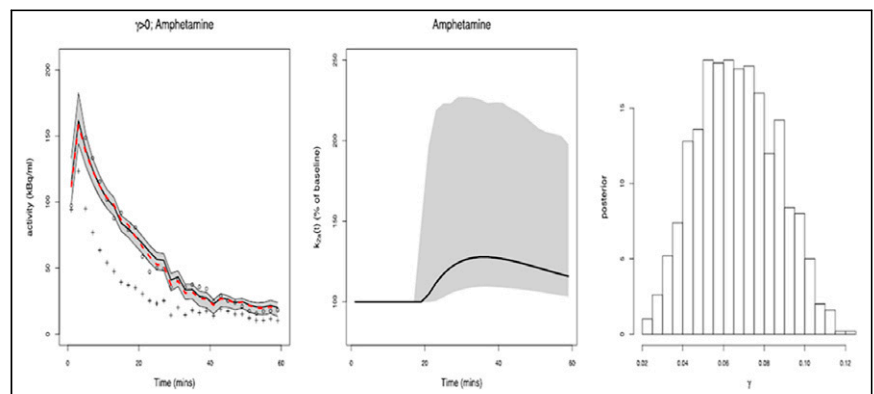


FIGURE 7. (Left) Measured $[^{11}\text{C}]\text{raclopride}$ time–activity curve for striatum (\circ) and cerebellum ($+$) of awake rat who received amphetamine at 20 min (activity in kBq/mL, time in min), along with PET-ABC–estimated time–activity curve (solid curve) and 95% CI (shaded area). (Middle) Estimated dopamine curve ($k_{2a}(t)$ in % of baseline) with 95% CI (shaded area). (Right) Posterior probability distribution for lp-ntPET model parameter, γ . (Adapted with permission of (66).)

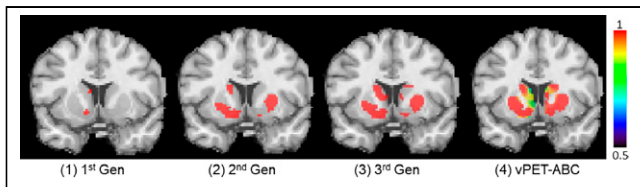


FIGURE 8. Activation (red) detected at voxel level in dynamic raclopride images of cigarette smoking in scanner by first generation (LSRRM), second generation (lp-ntPET), and third generation (lp-ntPET with adaptive model comparison; reprinted from (54)). Rightmost panel is result of lp-ntPET embedded in vPET-ABC framework, with threshold for activation set to 0.5; this panel is displayed as probability of activation map (color scale shows probability values ranging from 0.5 to 1) for single subject rather than as binary activation map. Gen = generation. (Reprinted from (56).)

PET-ABC gives a complete view of the reliability of parameter estimates by providing posterior probability distributions of each model parameter, from which one can derive the mean, median, and mode and their credible intervals. For example, the posterior probability distribution for the activation magnitude, γ , is shown in Figure 7 for an amphetamine challenge study conducted on an awake rat (49). The posterior distribution gives an indication of the confidence that can be placed in the value of γ .

The PET-ABC method has been adapted by Grazian et al. (67) to enable voxel-based analysis (vPET-ABC) by leveraging a high degree of parallelization of the algorithm. Another feature of the PET-ABC method is that one can perform model selection, in which alternative models are probabilistically evaluated for their ability to describe a given dataset. In the case of PET neurotransmitter activation studies, one can test the credibility of a detected activation by assessing the posterior probabilities of lp-ntPET versus the more parsimonious model, MRTM.

vPET-ABC can add value to lp-ntPET by virtue of its estimation of the posterior probability distribution for each model parameter, which is a way to assess confidence in our parameter estimates based on single-subject data. In addition to producing a posterior distribution for each model parameter (including the activation magnitude, γ), it also produces a probability of activation at every voxel. Therefore, we can enrich the information in the binary activation maps of the single individual shown in Figure 4B to produce a probabilistic map of activation in that same individual by mapping the posterior of the model selection parameter at every voxel (Fig. 8) (56). Knowing the level of certainty of the activation pattern is an added value provided by such methods, especially when analyzing single-subject data.

FUTURE CHALLENGES

There remain challenges to the proliferation and widespread adoption of lp-ntPET and other time-variant models for the analysis of non-steady state PET data. The challenges can be grouped into 3 overlapping domains: temporal accuracy, signal-to-noise ratio, and molecular and physiologic generalizability.

The temporal accuracy of the functions that describe the transient activation is needed to reliably differentiate activation phenomena that differ in timing. Said another way, the timing parameters of any time-varying model must be identifiable. For example, if the peak time of dopamine release is altered slightly by a drug, and this alteration is important medically, the estimate of peak time must be precise enough to establish significant differences between groups. It is worth noting that Normandin et al. (42) adopted a particular

formulation of the γ -variate as a basis function (first introduced by Madsen (44)) specifically because it decoupled peak time from take-off time.

Achieving better temporal accuracy can be thought of as a modeling problem. To date, the basis functions have been γ -variates because the stimuli have mostly been discrete in time and very little is known about the shape of the response curves. Best to keep it simple. But there is nothing to keep us from using more complicated basis functions—other than the increased risk that comes with more parameters and a greater likelihood of correlation between parameters. If, however, an activation was known to be, for example, bimodal, a function other than a γ -variate might be preferable.

As discussed, false-positive detection of activation is driven in large part by noise in the time-activity curves. Many types of analyses (that we refer to as third generation) have been introduced to reduce the noise—that is, to increase the ratio of dopamine signal to PET noise. At the same time, the noise problem is being attacked through the development of ultra-high-sensitivity PET scanners. Whole-body scanners with longer axial fields of view have much greater geometric sensitivity than previous generations of scanners and, therefore, capture much more of the emitted radiation (68). The result is substantially higher imaging performance, particularly an improved signal-to-noise ratio throughout the body (69,70). Similarly, the newest generation of ultra-high-sensitivity brain scanner is an order of magnitude more sensitive (71) than the best previous brain-dedicated machine, the Siemens HRRT. A simulation study by Liu and Morris (72) indicated that even a 10-times increase in sensitivity to coincidences would greatly improve the ability of lp-ntPET to differentiate early from late dopamine responses. Figure 9 demonstrates that the combination of increased sensitivity to coincidences with a nearest-neighbor clustering algorithm performs markedly better than the HRRT (and similar clustering) at identifying transient dopamine activation in voxel-level time-activity curves. Continued innovations in physics and engineering that result in even higher signal-to-noise ratios (e.g., as a result of improved time-of-flight resolution) should lead to yet more reliable detection and classification of activation events of very low magnitude.

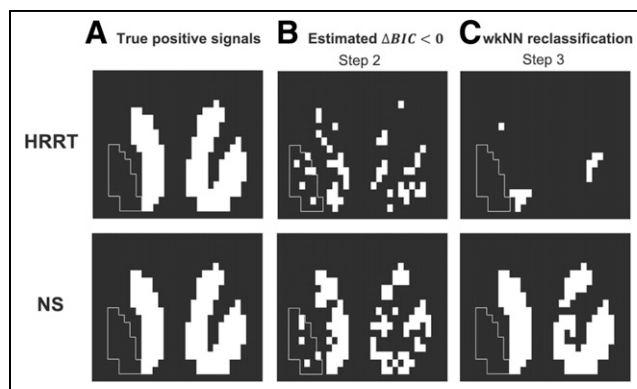


FIGURE 9. Third-generation performance: voxels with significant responses after applying steps 2 and 3 of nearest-neighbor clustering algorithm (as described in (72)) to phantom data simulated to reflect sensitivity of HRRT scanner and phantom data simulated to reflect sensitivity of newest generation scanner (NS). (A) True positive voxels in 1 slice of 3-dimensional phantom resembling striatum. (B) Voxels in which activation is detected by lp-ntPET. (C) Reclassified voxels after applying nearest-neighbor clustering to B. White outline delineates left putamen, which was simulated to represent raclopride data without any dopamine activation. (Reprinted with permission of (72).)

High-sensitivity whole-body PET scanners, when coupled with advanced time-varying models, also open up the possibility of studying signaling between the brain and peripheral organs—in other words, studies of neurochemical connectivity, as defined by Liu and Morris (72). Such studies will require not only high sensitivity and careful experimental design but also methods that go beyond the detection of isolated clusters of activated voxels, that is, methods that are capable of characterizing distributed networks of connected activations in terms of their correlations in space and time. The Bayesian methodology provides a natural framework for analyzing such correlations, but there is also a body of well-studied network-based statistical methods arising from the literature on MRI-based functional and structural connectivity that PET researchers can draw on (e.g., Sala et al. (73)).

For the most part, this review has focused on dopamine. The simple fact is that most successful studies of neurotransmitter activation have been with [¹¹C]raclopride. Raclopride has been shown to be ideally suited, kinetically, to the detection of dopamine transients (20). An essential quality of raclopride is its dissociation rate constant. Raclopride dissociates sufficiently rapidly in the presence of a transient increase in its competitor, dopamine. Unfortunately, to date, most high-affinity ligands (e.g., [¹⁸F]-fallypride) achieve their great affinity for the dopamine receptor via slow dissociation, which makes them less than maximally responsive to abrupt changes in dopamine. Going forward, there are 2 challenges for chemistry. The first is to create more displaceable tracers for more neurotransmitter systems, and the second is to achieve high affinity through increased rate constants of association rather than slower dissociation. This is the gauntlet we throw down before our drug development and radiochemistry colleagues.

We have come a long way since the days of treating the changing state of the brain's neurochemistry during PET imaging studies as an experimental confound to be avoided. Now, not only do we recognize the nonsteady state as an important phenomenon worthy of study, but we also have the data analysis methods and instruments to do so. Yet, we have barely scratched the surface. Further innovations in time-varying modeling and PET sensitivity (as suggested by simulations) will surely enable better characterization of the location, timing, and shape of neurotransmitter responses to specific interventions. All of this, we believe, will help untangle the mechanisms of neurochemical signaling within the brain—and between the brain and the peripheral organs—that regulate our responses to a changing environment. The future is bright and unsteady.

DISCLOSURE

No potential conflict of interest relevant to this article was reported.

REFERENCES

- Volkow ND, Swanson JM. Variables that affect the clinical use and abuse of methylphenidate in the treatment of ADHD. *Am J Psychiatry*. 2003;160:1909–1918.
- Manza P, Tomasi D, Shokri-Kojori E, et al. Neural circuit selective for fast but not slow dopamine increases in drug reward. *Nat Commun*. 2023;14:6408.
- Tomasi D, Manza P, Logan J, et al. Time-varying SUVR reflects the dynamics of dopamine increases during methylphenidate challenges in humans. *Commun Biol*. 2023;6:166.
- Rollema H, Coe JW, Chambers LK, Hurst RS, Stahl SM, Williams KE. Rationale, pharmacology and clinical efficacy of partial agonists of $\alpha_4\beta_2$ nACh receptors for smoking cessation. *Trends Pharmacol Sci*. 2007;28:316–325.

- Jedema HP, Narendran R, Bradberry CW. Amphetamine-induced release of dopamine in primate prefrontal cortex and striatum: striking differences in magnitude and timecourse. *J Neurochem*. 2014;130:490–497.
- Narendran R, Jedema HP, Lopresti BJ, et al. Imaging dopamine transmission in the frontal cortex: a simultaneous microdialysis and [¹¹C]FLB 457 PET study. *Mol Psychiatry*. 2014;19:302–310.
- Yoder KK, Wang C, Morris ED. Change in binding potential as a quantitative index of neurotransmitter release is highly sensitive to relative timing and kinetics of the tracer and the endogenous ligand. *J Nucl Med*. 2004;45:903–911.
- Sullivan JM, Kim SJ, Cosgrove KP, Morris ED. Limitations of SRTM, Logan graphical method, and equilibrium analysis for measuring transient dopamine release with [¹¹C]raclopride PET. *Am J Nucl Med Mol Imaging*. 2013;3:247–260.
- Fox PT, Mintun MA, Raichle ME, Herscovitch P. A noninvasive approach to quantitative functional brain mapping with H₂¹⁵O and positron emission tomography. *J Cereb Blood Flow Metab*. 1984;4:329–333.
- Wagner HN Jr, Burns HD, Dannals RF, et al. Imaging dopamine receptors in the human brain by positron tomography. *Science*. 1983;221:1264–1266.
- Garnett ES, Firmau G, Nahmias C. Dopamine visualized in the basal ganglia of living man. *Nature*. 1983;305:137–138.
- Mintun MA, Raichle ME, Kilbourn MR, Wooten GF, Welch MJ. A quantitative model for the in vivo assessment of drug binding sites with positron emission tomography. *Ann Neurol*. 1984;15:217–227.
- Logan J, Wolf AP, Shiue CY, Fowler JS. Kinetic modeling of receptor-ligand binding applied to positron emission tomographic studies with neuroleptic tracers. *J Neurochem*. 1987;48:73–83.
- Koepp MJ, Gunn RN, Lawrence AD, et al. Evidence for striatal dopamine release during a video game. *Nature*. 1998;393:266–268.
- Logan J, Dewey SL, Wolf AP, et al. Effects of endogenous dopamine on measures of [¹⁸F]N-methylspiperidol binding in the basal ganglia: comparison of simulations and experimental results from PET studies in baboons. *Synapse*. 1991;9:195–207.
- Fisher RE, Morris ED, Alpert NM, Fischman AJ. In vivo imaging of neuromodulatory synaptic transmission using PET: a review of relevant neurophysiology. *Hum Brain Mapp*. 1995;3:24–34.
- Morris ED, Fisher RE, Alpert NM, Rauch SL, Fischman AJ. In vivo imaging of neuromodulation using positron emission tomography: optimal ligand characteristics and task length for detection of activation. *Hum Brain Mapp*. 1995;3:35–55.
- Malizia AFK, Gunn R, Cunningham VJ, Wilson S, Jones T, Nutt DJ. The analysis of brain radioligand displacement studies. In: Myers R CV, Bailey D, Jones T, eds. *Quantification of Brain Function Using PET*. Academic Press; 1996:266–270.
- Endres CJ, Carson RE. Assessment of dynamic neurotransmitter changes with bolus or infusion delivery of neuroreceptor ligands. *J Cereb Blood Flow Metab*. 1998;18:1196–1210.
- Morris ED, Yoder KK. Positron emission tomography displacement sensitivity: predicting binding potential change for positron emission tomography tracers based on their kinetic characteristics. *J Cereb Blood Flow Metab*. 2007;27:606–617.
- Alpert NM, Badgaiyan RD, Livni E, Fischman AJ. A novel method for noninvasive detection of neuromodulatory changes in specific neurotransmitter systems. *Neuroimage*. 2003;19:1049–1060.
- Gunn RN, Lammertsma AA, Hume SP, Cunningham VJ. Parametric imaging of ligand-receptor binding in PET using a simplified reference region model. *Neuroimage*. 1997;6:279–287.
- Lammertsma AA, Hume SP. Simplified reference tissue model for PET receptor studies. *Neuroimage*. 1996;4:153–158.
- Ichise M, Liow JS, Lu JQ, et al. Linearized reference tissue parametric imaging methods: application to [¹¹C]DASB positron emission tomography studies of the serotonin transporter in human brain. *J Cereb Blood Flow Metab*. 2003;23:1096–1112.
- Badgaiyan RD, Fischman AJ, Alpert NM. Dopamine release during human emotional processing. *Neuroimage*. 2009;47:2041–2045.
- Christian BT, Lehrer DS, Shi B, et al. Measuring dopamine neuromodulation in the thalamus: using [F-18]fallypride PET to study dopamine release during a spatial attention task. *Neuroimage*. 2006;31:139–152.
- Kasanova Z, Ceccarini J, Frank MJ, et al. Daily-life stress differentially impacts ventral striatal dopaminergic modulation of reward processing in first-degree relatives of individuals with psychosis. *Eur Neuropsychopharmacol*. 2018;28:1314–1324.
- Kasanova Z, Ceccarini J, Frank MJ, et al. Intact striatal dopaminergic modulation of reward learning and daily-life reward-oriented behavior in first-degree relatives of individuals with psychotic disorder. *Psychol Med*. 2018;48:1909–1914.
- Lataster J, Collip D, Ceccarini J, et al. Psychosocial stress is associated with in vivo dopamine release in human ventromedial prefrontal cortex: a positron emission tomography study using [¹⁸F]fallypride. *Neuroimage*. 2011;58:1081–1089.
- Lataster J, Collip D, Ceccarini J, et al. Familial liability to psychosis is associated with attenuated dopamine stress signaling in ventromedial prefrontal cortex. *Schizophr Bull*. 2014;40:66–77.
- Ros T, Kwiek J, Andriot T, et al. PET imaging of dopamine neurotransmission during EEG neurofeedback. *Front Physiol*. 2021;11:590503.

32. Vrieze E, Ceccarini J, Pizzagalli DA, et al. Measuring extrastriatal dopamine release during a reward learning task. *Hum Brain Mapp.* 2013;34:575–586.
33. Zakiniaez Y, Liu H, Gao H, et al. Nicotine patch alters patterns of cigarette smoking-induced dopamine release: patterns relate to biomarkers associated with treatment response. *Nicotine Tob Res.* 2022;24:1597–1606.
34. Dedovic K, Renwick R, Mahani NK, Engert V, Lupien SJ, Pruessner JC. The Montreal Imaging Stress Task: using functional imaging to investigate the effects of perceiving and processing psychosocial stress in the human brain. *J Psychiatry Neurosci.* 2005;30:319–325.
35. Nagano-Saito A, Dagher A, Booij L, et al. Stress-induced dopamine release in human medial prefrontal cortex: ^{18}F -fallypride/PET study in healthy volunteers. *Synapse.* 2013;67:821–830.
36. Liu H, Zakiniaez Y, Cosgrove KP, Morris ED. Toward whole-brain dopamine movies: a critical review of PET imaging of dopamine transmission in the striatum and cortex. *Brain Imaging Behav.* 2019;13:314–322.
37. Morris ED, Yoder KK, Wang C, et al. ntPET: a new application of PET imaging for characterizing the kinetics of endogenous neurotransmitter release. *Mol Imaging.* 2005;4:473–489.
38. Morris ED, Normandin MD, Schiffer WK. Initial comparison of ntPET with microdialysis measurements of methamphetamine-induced dopamine release in rats: support for estimation of dopamine curves from PET data. *Mol Imaging Biol.* 2008;10:67–73.
39. Constantinescu CC, Bouman C, Morris ED. Nonparametric extraction of transient changes in neurotransmitter concentration from dynamic PET data. *IEEE Trans Med Imaging.* 2007;26:359–373.
40. Constantinescu CC, Yoder KK, Kareken DA, et al. Estimation from PET data of transient changes in dopamine concentration induced by alcohol: support for a non-parametric signal estimation method. *Phys Med Biol.* 2008;53:1353–1367.
41. Normandin MD, Morris ED. Estimating neurotransmitter kinetics with ntPET: a simulation study of temporal precision and effects of biased data. *Neuroimage.* 2008;39:1162–1179.
42. Normandin MD, Schiffer WK, Morris ED. A linear model for estimation of neurotransmitter response profiles from dynamic PET data. *Neuroimage.* 2012;59:2689–2699.
43. Morris ED, Constantinescu CC, Sullivan JM, Normandin MD, Christopher LA. Noninvasive visualization of human dopamine dynamics from PET images. *Neuroimage.* 2010;51:135–144.
44. Madsen MT. A simplified formulation of the gamma variate function. *Phys Med Biol.* 1992;37:1597.
45. Gunn RN, Gunn SR, Turkheimer FE, Aston JA, Cunningham VJ. Positron emission tomography compartmental models: a basis pursuit strategy for kinetic modeling. *J Cereb Blood Flow Metab.* 2002;22:1425–1439.
46. Perkins KA, Gerlach D, Vender J, Grobe J, Meeker J, Hutchison S. Sex differences in the subjective and reinforcing effects of visual and olfactory cigarette smoke stimuli. *Nicotine Tob Res.* 2001;3:141–150.
47. Cosgrove KP, Wang S, Kim SJ, et al. Sex differences in the brain's dopamine signature of cigarette smoking. *J Neurosci.* 2014;34:16851–16855.
48. Calakos KC, Liu H, Lu Y, et al. Assessment of transient dopamine responses to smoked cannabis. *Drug Alcohol Depend.* 2021;227:108920.
49. Kyme AZ, Angelis GI, Eisenhuth J, et al. Open-field PET: simultaneous brain functional imaging and behavioural response measurements in freely moving small animals. *Neuroimage.* 2019;188:92–101.
50. Kim SJ, Sullivan JM, Wang S, Cosgrove KP, Morris ED. Voxelwise lp-ntPET for detecting localized, transient dopamine release of unknown timing: sensitivity analysis and application to cigarette smoking in the PET scanner. *Hum Brain Mapp.* 2014;35:4876–4891.
51. Christian BT, Vandehey NT, Floberg JM, Mistretta CA. Dynamic PET denoising with HYPR processing. *J Nucl Med.* 2010;51:1147–1154.
52. Wang S, Kim S, Cosgrove KP, Morris ED. A framework for designing dynamic lp-ntPET studies to maximize the sensitivity to transient neurotransmitter responses to drugs: application to dopamine and smoking. *Neuroimage.* 2017;146:701–714.
53. Akaike H. A new look at the statistical model identification. *IEEE Trans Automat Contr.* 1974;19:716–723.
54. Liu H, Morris ED. Model comparison metrics require adaptive correction if parameters are discretized: proof-of-concept applied to transient signals in dynamic PET. *IEEE Trans Med Imaging.* 2020;39:2451–2460.
55. Angelis GI, Fuller OK, Gillam JE, Meikle SR. Denoising non-steady state dynamic PET data using a feed-forward neural network. *Phys Med Biol.* 2021;66:034001.
56. Emvalomenos GM, Hoyer J, Meikle SR, Morris ED. Sensitivity analysis for parametric imaging of subtle dopamine release using time-varying models: proof-of-concept in human smoking positron emission tomography data. Presented at: XIV International Symposium on Functional Neuroreceptor Mapping of the Living Brain; May 19, 2024; Montreal, Canada.
57. Angelis GI, Gillam JE, Ryder WJ, Fulton RR, Meikle SR. Direct estimation of voxel-wise neurotransmitter response maps from dynamic PET data. *IEEE Trans Med Imaging.* 2019;38:1371–1383.
58. Fuller OK, Angelis GI, Meikle SR. Classification of neurotransmitter response in dynamic PET data using machine learning approaches. *IEEE Trans Radiat Plasma Med Sci.* 2020;4:708–719.
59. Bevington CW, Cheng JK, Klyuzhin IS, Cherkasova MV, Winstanley CA, Sossi V. A Monte Carlo approach for improving transient dopamine release detection sensitivity. *J Cereb Blood Flow Metab.* 2021;41:116–131.
60. Klyuzhin IS, Bevington CWJ, Cheng JK, Sossi V. Detection of transient neurotransmitter response using personalized neural networks. *Phys Med Biol.* 2020;65:235004.
61. Bevington CW, Hanania JU, Ferrareso G, et al. Novel voxelwise residual analysis of $^{[11\text{C}]}$ raclopride PET data improves detection of low-amplitude dopamine release. *J Cereb Blood Flow Metab.* 2024;44:757–771.
62. Malave P, Sitek A. Bayesian analysis of a one compartment kinetic model used in medical imaging. *J Appl Stat.* 2015;42:98–113.
63. Zhou Y, Aston JAD, Johansen AM. Bayesian model comparison for compartmental models with applications in positron emission tomography. *J Appl Stat.* 2013;40:993–1016.
64. Irace Z, Merida I, Redoute J, et al. Bayesian estimation of the ntPET model in single-scan competition PET studies. *Front Physiol.* 2020;11:498.
65. Fan Y, Meikle SR, Angelis G, Sitek A. ABC in nuclear imaging. In: Sisson SA, Fan Y, Beaumont MA, eds. *Handbook of Approximate Bayesian Computation.* Chapman & Hall/CRC Press.; 2018:623–648.
66. Fan Y, Emvalomenos G, Grazian C, Meikle SR. fully Bayesian likelihood-free inference for kinetic models. *Phys Med Biol.* 2021;66.
67. Grazian C, Emvalomenos G, Angelis G, Fan Y, Meikle SR. PET-ABC: voxel-wise approximate bayesian inference for parametric imaging of neurotransmitter release. Paper presented at: 2021 IEEE Nuclear Science Symposium and Medical Imaging Conference (NSS/MIC); October 16–23, 2021; Piscataway, NJ.
68. Pantel AR, Mankoff dopamine, Karp JS. Total-body PET: will it change science and practice? *J Nucl Med.* 2022;63:646–648.
69. Prenosil GA, Sari H, Furstner M, et al. Performance characteristics of the Biograph Vision Quadra PET/CT system with a long axial field of view using the NEMA NU 2-2018 standard. *J Nucl Med.* 2022;63:476–484.
70. Spencer BA, Berg E, Schmall JP, et al. Performance evaluation of the uEXPLORER total-body PET/CT scanner based on NEMA NU 2-2018 with additional tests to characterize PET scanners with a long axial field of view. *J Nucl Med.* 2021;62:861–870.
71. Li H, Badawi RD, Cherry SR, et al. Performance characteristics of the NeuroEXPLORER, a next-generation human brain PET/CT imager. *J Nucl Med.* 2024;65:1320–1326.
72. Liu H, Morris ED. Detecting and classifying neurotransmitter signals from ultra-high sensitivity PET data: the future of molecular brain imaging. *Phys Med Biol.* 2021;66.
73. Sala A, Lizarraga A, Caminiti SP, et al. Brain connectomics: time for a molecular imaging perspective? *Trends Cogn Sci.* 2023;27:353–366.
74. Innis RB, Cunningham VJ, Delforge J, et al. Consensus nomenclature for in vivo imaging of reversibly binding radioligands. *J Cereb Blood Flow Metab.* 2007;27:1533–1539.